Available online at www.sciencedirect.com
ScienceDirect
Trans. Nonferrous Met. Soc. China 32(2022) 1650−1663
Transactions of Nonferrous Metals Society of China
www.tnmsc.cn

Effect of temperature, oxygen partial pressure and calcium lignosulphonate on chalcopyrite dissolution in sulfuric acid solution

Yun-long BAI[1,2], Wei WANG[1,2], Feng XIE[1,2], Dian-kun LU[1,2], Kai-xi JIANG[3]

1. Key Laboratory for Ecological Metallurgy of Multimetallic Ores (Ministry of Education), Northeastern University, Shenyang 110819, China;
2. School of Metallurgy, Northeastern University, Shenyang 110819, China;
3. College of Zijin Mining, Fuzhou University, Fuzhou 350108, China

Received 25 March 2021; accepted 10 September 2021

Abstract: The pressure leaching mechanism of chalcopyrite was studied by both leaching tests and in-situ electrochemical measurements. The effects of leaching temperature, oxygen partial pressure, and calcium lignosulphonate, on copper extraction and iron extraction of chalcopyrite pressure leaching were investigated. The leaching rate is accelerated by increasing the leaching temperature from 120 to 150 °C and increasing oxygen partial pressure to 0.7 MPa. The release of iron is faster than that of copper due to the formation of iron-depleted sulfides. Under the optimal leaching conditions without calcium lignosulphonate, the copper and iron extraction rates are 79% and 81%, respectively. The leaching process is mixedly controlled by surface reaction and product layer diffusion with an activation energy of 36.61 kJ/mol. Calcium lignosulphonate can effectively remove the sulfur passive layer, and the activation energy is 45.59 kJ/mol, suggesting that the leaching process with calcium lignosulphonate is controlled by surface chemical reactions. Elemental sulfur is the main leaching product, which is mixed with iron-depleted sulfides and leads to the passivation of chalcopyrite. Electrochemical studies suggest that increasing the oxygen partial pressure leads to increasing the cathodic reaction rate and weakening the passivation of chalcopyrite.
Key words: chalcopyrite; pressure-oxidative leaching; calcium lignosulphonate; kinetics; electrochemistry

1 Introduction

The copper demand has dramatically increased in recent decades and this situation may continue until 2050 [1,2]. Most of the copper ore deposits belong to sulfide minerals (e.g. $CuFeS_2$, Cu_5FeS_4, $CuFeS_2$ and Cu_2S). Chalcopyrite is one of the most abundant and refractory minerals. Currently, about 80% copper is produced by pyrometallurgical technology. The formation of sulfur dioxide during pyrometallurgical processes has a serious impact on environmental protection, and governments are tightening environmental restrictions to control the sulfur dioxide emission. In contrast, hydrometallurgical technology has been considered to be a promising alternative for extracting copper from chalcopyrite, due to its cost-effectiveness and environmental friendliness [3,4].

Treating chalcopyrite by hydrometallurgical technology has attracted great attention, and the chalcopyrite leaching kinetics was studied in various leaching media such as iron sulfate [5,6], hydrochloric acid [7], methanesulfonic acid [8] and hypochlorite solution [9]. However, the sluggish leaching kinetics and high activation energy hinder the commercial application of hydrometallurgical process [8]. The mechanisms of

Corresponding author: Wei WANG, Tel: +86-24-83672298, E-mail: wangwei@smm.neu.edu.cn;
Feng XIE, Tel: +86-24-83672298, E-mail: xief@smm.neu.edu.cn
DOI: 10.1016/S1003-6326(22)65900-4

active−passive and passive−transpassive transitions of chalcopyrite are still ambiguous [10,11]. The passive behavior of chalcopyrite leaching was reported to be caused by the passive layers, such as element sulfur [12], polysulfide [13] and jarosite [12,14], or the electronic structure of chalcopyrite [15,16].

In order to improve the chalcopyrite leaching kinetics, extensive research has been carried out, such as atmospheric-oxidation [8,17], pressure-oxidation [18,19] and bio-oxidation [14]. Despite the preliminary success achieved by the methods mentioned, the copper extraction was still unsatisfactory due to the fast decomposition of oxidant or the formation of surface passive layer. An apparent activation energy of chalcopyrite leaching with hydrogen peroxide was calculated to be 19.6 kJ/mol, which suggested that the leaching process was controlled by the surface layer(s) [20]. Pressure-oxidative leaching has been considered to be an effective method for extracting copper from chalcopyrite. According to the open literature, pressure-oxidative leaching can improve the leaching efficiency, and also provide a favorable condition to form sulfate [21,22]. Table 1 summarizes the leaching products of chalcopyrite in different leaching medium and temperature range.

Table 1 Leaching products of chalcopyrite in different leaching media and temperature ranges

Medium	Temperature range/°C	Leaching product	Ref.
$H_2SO_4 + O_2$	125−175	Sulfate + S^0	[23]
$H_2SO_4 + O_2$	160−180	$Fe_2O_3 + H_2SO_4$	[24]
$C_2H_2O_4 + O_2$	45−175	$CuC_2O_4 + Fe_2O_3$	[22]
$H_2SO_4 + O_2$	110	S^0	[18]

Reactions (1)−(5) were used to describe the pressure-oxidative leaching processes of chalcopyrite [19,21,22]:

$$2CuFeS_2+2.5O_2+5H_2SO_4 \rightarrow 2CuSO_4+Fe_2(SO_4)_3+4S^0+5H_2O \quad (1)$$

$$CuFeS_2+2Fe_2(SO_4)_3 \rightarrow CuSO_4+5FeSO_4+2S^0 \quad (2)$$

With increasing the oxygen partial pressure, elemental sulfur can be converted to sulfuric acid, and ferrous sulfate can be oxidized to ferric sulfate:

$$2S^0+3O_2+2H_2O \rightarrow 2H_2SO_4 \quad (3)$$

$$2FeSO_4+0.5O_2+H_2SO_4 \rightarrow Fe_2(SO_4)_3+H_2O \quad (4)$$

Therefore, the processes of chalcopyrite dissolution can also be presented by

$$2CuFeS_2+8.5O_2+H_2SO_4 \rightarrow 2CuSO_4+Fe_2(SO_4)_3+5H_2O \quad (5)$$

$$2CuFeS_2+16Fe_2(SO_4)_3+H_2O \rightarrow 2CuSO_4+34FeSO_4+16H_2SO_4 \quad (6)$$

Although the above chemical reactions could describe the chalcopyrite dissolution process well, they did not provide the information about the surface passive layer formation. Depending on the acidity of medium, ferric sulfate can be transformed to hematite, hydronium jarosite, or basic ferric sulfate, which are considered to be one of the components of the surface passive layer [24].

Based on the leaching temperature, pressure leaching of chalcopyrite can be classified into three types: low (<100 °C), medium (100−180 °C) and high-temperature (>200 °C) [25]. Leaching chalcopyrite at medium-temperature (100−180 °C) is preferred to the other two types with regard to the production of acid wastewater and the demanding for higher oxygen consumption [21,25]. Chalcopyrite pressure leaching at medium-temperature has received great attention. However, the leaching mechanism was almost studied by ex-situ methods, such as conventional leaching tests and ex-situ spectroscopic methods. These ex-situ methods have their advantages, but they are unable to detect instantly the response of solid−liquid interface information during the leaching processes [26]. Electrochemical techniques, as an effective in-situ research method, have been widely applied to understanding the leaching mechanism of chalcopyrite [27,28]. However, investigations of the electrochemical mechanisms of chalcopyrite leaching were carried out under ambient temperature conditions, and to the authors' knowledge, few electrochemical studies on pressure leaching of chalcopyrite have been published [26].

In this study, the leaching kinetics and the electrochemical mechanism of chalcopyrite pressure leaching in sulfuric acid solution at a temperature ranging from 110 to 150 °C were investigated. The effects of temperature, oxygen partial pressure and calcium lignosulphonate on chalcopyrite pressure leaching were investigated. X-ray diffraction (XRD), scanning electron

microscopy (SEM), electron microprobe and X-ray photoelectron spectroscopy (XPS) were used to study the surface chemical statues and the morphology of the leaching residues. In-situ electrochemical measurements were carried out to further understand the electrochemical mechanism of chalcopyrite pressure leaching.

2 Experimental

2.1 Materials

The chalcopyrite ore used in this study was obtained from a mine in Guangxi, China. The chalcopyrite ore was first crushed by a jaw crusher, and then dried at 45 °C in a drying oven for 12 h. According to results of screening testing, the ore used for leaching experiment has the particle size of 90% passing 75 μm and 50% passing 38 μm, respectively. The chemical composition of chalcopyrite was determined by chemical titration method as 32.60 wt.% Cu, 36.60 wt.% S, and 22.63 wt.% Fe. The phase composition was determined by the X-ray diffraction (XRD) analysis, as shown in Fig. 1, suggesting that the ore was composed of a well-crystallized chalcopyrite. The chemical reagents used in all experiments were of analytical grade.

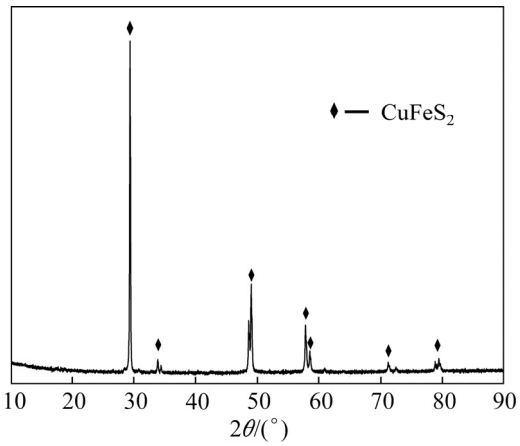

Fig. 1 XRD pattern of chalcopyrite ore

2.2 Leaching experiment

The leaching experiments were carried out in a titanium autoclave (KCFD1−10, Keli Automatic Control Equipment Research Institute, China). For each leaching experiment, 5 g of chalcopyrite was leached with 500 mL lixiviant with mechanical agitation at the speed of 550 r/min. To avoid the oxidation of chalcopyrite during the heating processes, the air in autoclave was exhausted out by highly purified nitrogen gas before heating. When the system was heated to the set temperature, the highly purified oxygen gas was injected to maintain the required partial oxygen pressure. After pressure leaching, the container was rapidly cooled in air. The slurry was immediately filtered to obtain the pregnant leaching solution (PLS) and leaching residue. The obtained leaching residue was dried at 45 °C for 24 h prior to further analysis.

2.3 Analysis

The phases of the chalcopyrite and leaching residue were analyzed by X-ray diffraction (XRD: Cu $K_{\alpha 1}$, D8 Advance, Bruker, Germany). The morphology of samples was determined using field emission scanning electron microscopy (SEM: Zeiss UltraPlus, Germany). X-ray photoelectron spectroscopy (XPS) was used to study the chemical composition on the surface of minerals. The concentrations of copper and iron in the pregnant leaching solution were measured by an atomic absorption spectrophotometer (AA240FS, Agilent Technologies Inc, Santa Clara, CA, USA). The metal extraction (A) was calculated using Eq. (7):

$$A=\frac{C_\alpha \cdot V_\alpha}{C_\beta \cdot m_\beta}\times 100\% \tag{7}$$

where C_α and C_β are the concentration of metal in pregnant leaching solution (mg/L) and the content of metal in chalcopyrite sample (mg/g), respectively; V_α is the volume of leaching solution (L) and m_β is the mass of chalcopyrite sample (g).

2.4 Electrochemical measurements

An autoclave system equipped with three electrodes was used to carry out the electrochemical experiments to understand the chalcopyrite pressure-dissolution mechanism, as shown in Fig. 2. The working electrode (WE) was prepared by sealing the bulk chalcopyrite in synthetic resin, leaving only one face with a geometry area of 1 cm^2 to contact with the leaching solution. A platinum wire was used as the counter electrode (CE). An external pressure balanced Ag/AgCl electrode was used as the reference electrode (RE). The electrolyte of the reference electrode was refreshed before each test to ensure the reproducibility. All potentials mentioned in this study was converted to the saturated hydrogen electrodes (SHE) at 25 °C

according to Eq. (8) [26,29]:

$$\Delta\varphi_{SHE}=\Delta\varphi_{obs}+286.6-\Delta T+1.745\times10^{-4}\Delta T^2-3.03\times10^{-6}\Delta T^3 \quad (8)$$

To avoid the formation of secondary minerals during the heating processes, the air was also exhausted out by highly purified nitrogen gas and only half of the electrolyte was pumped into the autoclave to avoid the contact of the working electrode and the electrolyte. When the system was heated to the required temperature, the remained electrolyte was pumped into the autoclave by a pressure pump. Electrochemical experiments were performed by using an electrochemical workstation controlled by VersaStudio Software (VersaSTAT.4). The open circuit potential (OCP) was recorded for a set time until the potential reached a quasi-steady state. Potentiodynamic tests were performed with a potential sweep rate of 1 mV/s. Electrochemical impedance spectroscopy (EIS) tests were carried out at open circuit potential (OCP) and the frequency was set in a range from 20 kHz to 0.1 Hz.

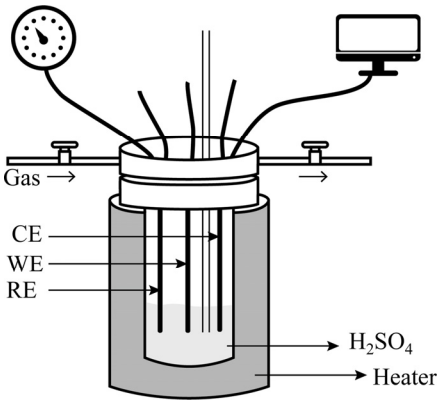

Fig. 2 Schematic illustration of electrochemical experiment system

3 Results and discussion

3.1 Effect of leaching temperature

To investigate the effect of leaching temperature on copper extraction and iron extraction, leaching tests were carried out at different temperatures of 110, 120, 130, 140 and 150 °C. The results of copper extraction and iron extraction are shown in Fig. 3. The copper extraction and iron extraction increased with prolonging leaching time at the first 120 min and then reached a quasi-stable status. When the leaching temperature was 110 °C, a final copper extraction of 60% was achieved, and the final iron extraction was close to 62%. It could be observed that increasing temperature from 110 to 120 °C had a negative influence on the chalcopyrite leaching, which might be caused by the physical state of elemental sulfur produced during the leaching process. The main leaching product of chalcopyrite under the studied conditions was elemental sulfur, which was detected by XRD and XPS. When the leaching temperature increased from 110 to 120 °C, solid elemental sulfur would be transferred to molten elemental sulfur. The molten sulfur had high viscosity and poor fluidity, forming a tighter product layer which hindered the contact of chalcopyrite and lixiviant. When the temperature increased from 130 to 150 °C, both copper extraction and iron extraction were increased as the leaching temperature increased.

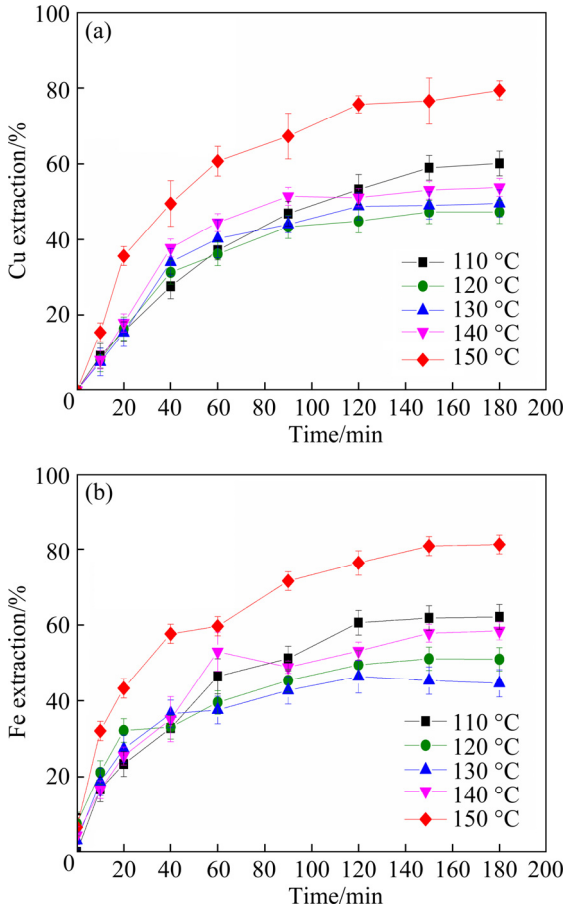

Fig. 3 Effect of leaching temperature on Cu (a) and Fe (b) extractions (H_2SO_4 concentration: 1.0 mol/L; partial oxygen pressure: 0.4 MPa; stirring speed: 550 r/min)

At the initial leaching stage (0−20 min), the extraction of iron was always higher than that of copper, indicating the faster release of iron into

solution. Based on the reported data, the potential required for chalcopyrite to be oxidized to Cu^{2+} is at least 0.137 V higher than that for oxidation to secondary minerals ($Cu_{1-x}S$ or Cu_5FeS_4), which means that oxidative reactions tend to form intermediates [30]. Additionally, the previous studies suggested that the iron-depleted sulfides were formed on the surfaces of chalcopyrite during leaching [6,31,32]. Therefore, the higher iron extraction rate at the initial leaching stage was caused by the formation of intermediate layers.

3.2 Effect of oxygen partial pressure

To investigate the effect of oxygen partial pressure on chalcopyrite leaching, leaching tests were carried out at the oxygen partial pressure ranging from 0.2 to 0.7 MPa, as shown in Fig. 4. Copper extraction increased with the increase of oxygen partial pressure, and a final copper extraction of 85% was obtained at 0.7 MPa after leaching for 180 min. However, iron extraction was not significantly changed when the oxygen partial pressure increased from 0.2 to 0.7 MPa.

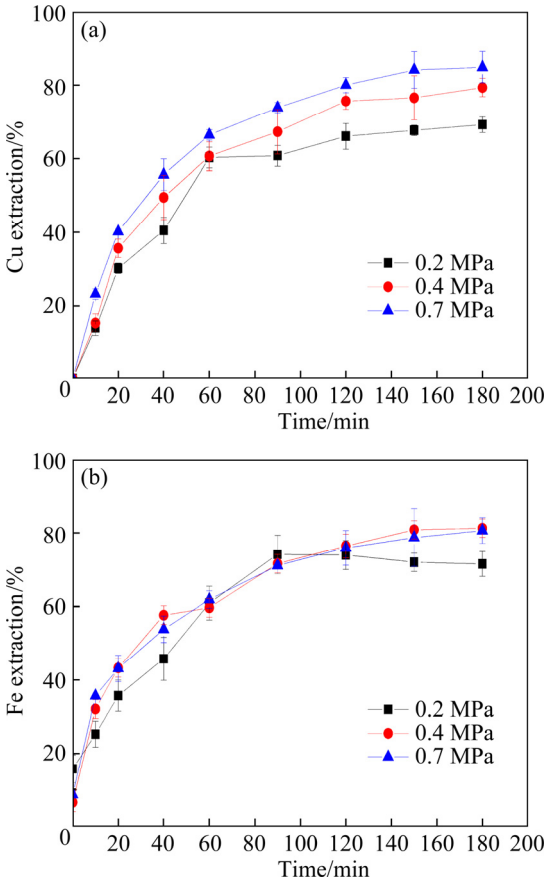

Fig. 4 Effect of oxygen partial pressure on Cu (a) and Fe (b) extractions (H_2SO_4 concentration: 1.0 mol/L; temperature: 150 °C; stirring speed: 550 r/min)

3.3 Effect of calcium lignosulphonate

Calcium lignosulphonate (CLS) is an environmentally friendly polyelectrolyte that contains aliphatic, aromatic, sulfonic, carboxylic and hydroxyl groups [33]. Calcium lignosulphonate was widely used as surfactant to maintain the rapid leaching kinetics [34,35]. HACKL et al [35] studied the feasibility of using calcium lignosulphonate to solve sulfur passivation layer in the temperature range from 125 to 155 °C, and the results showed that most of sulfur was rapidly dispersed and the copper extraction rate was increased [35].

To investigate the effect of calcium lignosulphonate on chalcopyrite leaching, tests were carried out at in 1.0 mol/L sulfuric acid solution with 0.2 g/L calcium lignosulphonate and 0.4 MPa of partial oxygen pressure in the temperature range of 110−150 °C, and the results are shown in Fig. 5. The increasing of leaching temperature had a significant influence on chalcopyrite dissolution in H_2SO_4−CLS mixed solution. At a lower temperature (110 °C), a final

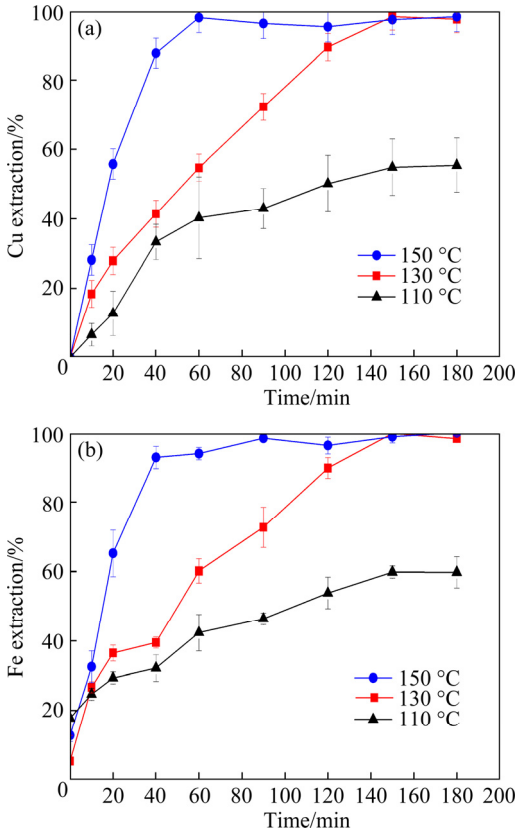

Fig. 5 Effect of leaching temperature on Cu (a) and Fe (b) extractions in H_2SO_4−CLS mixed solution (H_2SO_4 concentration: 1.0 mol/L; partial oxygen pressure: 0.4 MPa; CLS concentration: 0.2 g/L; stirring speed: 550 r/min)

copper extraction of 56% was obtained, and the copper extraction was closed to that without calcium lignosulfonate addition, suggesting that the calcium lignosulphonate had little influence on improving leaching efficiency when the temperature was below the melting point of sulfur. When the temperature was 130 °C, 98% of the chalcopyrite was dissolved in 150 min. When the leaching temperature further increased to 150 °C, chalcopyrite was rapidly dissolved, and about 98% of chalcopyrite was leached out within 60 min. These results were consistent with the previous report of chalcopyrite dissolution chemistry [35,36].

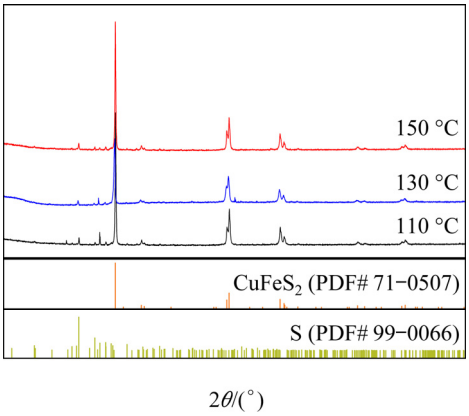

Fig. 6 XRD patterns of leaching residue obtained at 110, 130 and 150 °C

3.4 Leaching residue characterization

The phase compositions and the surface morphologies of leaching residue were investigated by XRD and SEM. As shown in Fig. 6, the un-leached chalcopyrite and elemental sulfur were the main phases for all the leaching residues, which further confirmed that elemental sulfur was the main leaching product, and the leaching process can be described as Reaction (1).

From the BSE images of the leaching residue, as shown in Fig. 7(a), the leaching residue of 110 °C was characterized by a particle size in the range of 4−180 μm with different shapes, and some conglomerates were formed. An inhomogeneous distribution of sulfur and un-leached chalcopyrite throughout the particles was also found, which could be related to the solid elemental sulfur. When the leaching temperature increased to higher than the melting point of elemental sulfur, the viscosity of the produced elemental sulfur increased and its fluidity became worse, which causes the particles of the leaching residue to become larger and form a smooth-surfaced conglomerate, as shown in Figs. 7(b, c). The particle size of the leaching residue obtained at 130 °C was between 0.8 and 2 mm, which was larger than that of the leaching residue obtained at 150 °C. This phenomenon could be related to the oxidation and dissolution of elemental sulfur. For the leaching residue obtained in H_2SO_4−CLS mixed solution, as shown in Figs. 7(d−f), the particles exhibited coarse surface with different shapes. As a result, the addition of calcium lignosulfonate could effectively disperse the surface molten sulfur and inhibit the formation of spherical particles, which enabled the mineral particles to maintain a large reaction surface area during leaching.

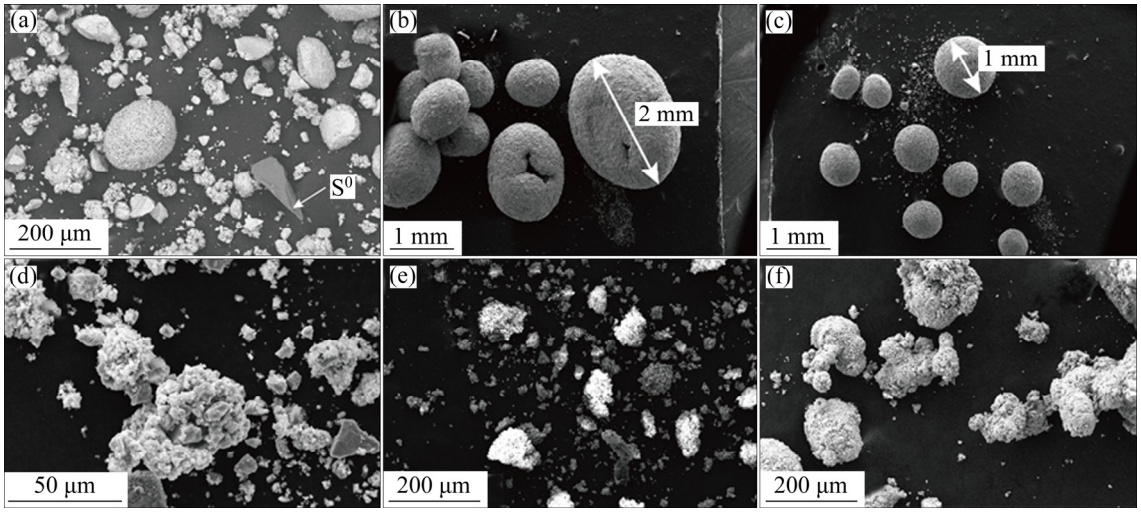

Fig. 7 SEM photographs of leaching residue obtained at 110 °C (a, d), 130 °C (b, e) and 150 °C (c, f) in H_2SO_4 solution (a−c), and in H_2SO_4−CLS mixed solution (d−f)

3.5 Kinetics study

According to above analysis, elemental sulfur was the main product under the study conditions. By assuming that the concentrations of sulfuric acid and chalcopyrite remained constant, the pressure leaching process can be described by different reaction models [20,37−39]. When the leaching process is controlled by chemical reactions, the integrated rate can be expressed as Eq. (9). If the process of chalcopyrite dissolution is under diffusion control, Eq. (10) can be chosen as the integral rate expression. If the pressure leaching process is mixed-controlled by the surface reaction and product layer diffusion, the integral rate expression is shown as Eq. (11):

$$1-(1-\alpha)^{1/3}=k_r t \quad (9)$$

$$1-2/3\alpha-(1-\alpha)^{2/3}=k_d t \quad (10)$$

$$1/3\ln(1-\alpha)+[(1-\alpha)^{-1/3}-1]=k_m t \quad (11)$$

where α is the fraction reacted, k_r, k_d and k_m are the kinetic constants and t is leaching time.

Based on the leaching results, the pressure leaching of chalcopyrite without calcium lignosulphonate was affected by leaching temperature and the product layer, and as a result the mixed kinetics model can be used to study the leaching process. For leaching chalcopyrite with calcium lignosulphonate, increasing temperature had a positive influence on leaching kinetics, and therefore the surface reaction model is suitable for studying the leaching process in H_2SO_4−CLS solution. The kinetics curves and the Arrhenius plots of ln k are shown in Figs. 8 and 9, respectively, which shows that the used models could describe the leaching kinetics well. As can be seen in Fig. 8, the activation energy in the temperature range of 120−140 °C was calculated to be 36.61 kJ/mol, which further supported the assumption that the

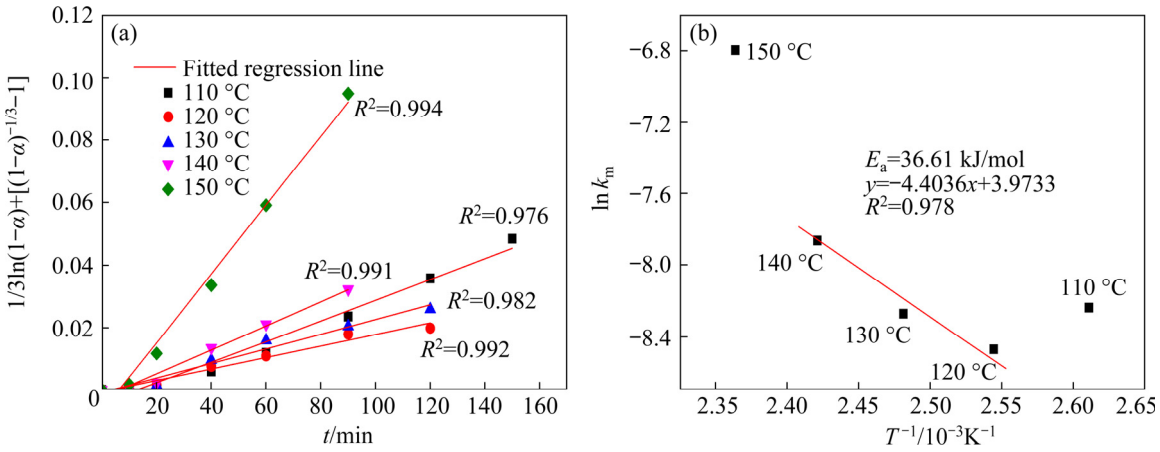

Fig. 8 Plot of $1/3\ln(1-\alpha)+[(1-\alpha)^{-1/3}-1]$ versus t (a) and Arrhenius plot (b) for chalcopyrite dissolution without calcium lignosulphonate at different temperatures

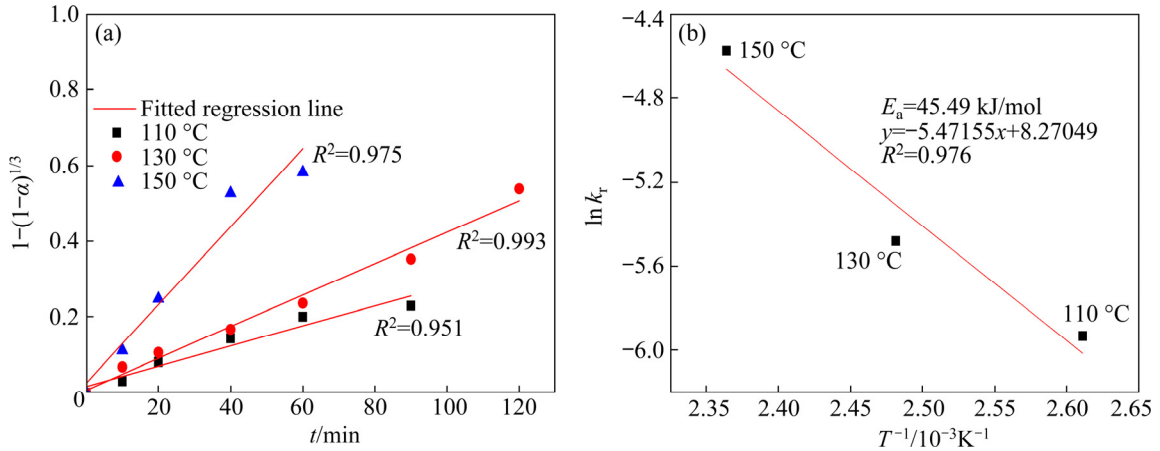

Fig. 9 Plot of $1-(1-\alpha)^{1/3}=k_r t$ versus t (a) and Arrhenius plot (b) for chalcopyrite dissolution with calcium lignosulphonate at different temperatures

pressure leaching process in H_2SO_4 solution was controlled by surface reaction and product layer diffusion. For pressure leaching chalcopyrite in H_2SO_4−CLS mixed solution, the copper leaching process followed the surface reaction controlling unreacted shrinking core mode, and an activation energy of 45.49 kJ/mol was obtained from the Arrhenius plots.

3.6 Electrochemical studies of chalcopyrite pressure leaching

3.6.1 Open circuit potential (OCP) and potentiodynamics studies

To further study the dissolution behavior and passivation phenomena of chalcopyrite, open circuit potential (OCP) tests and potentiodynamic tests were carried out in 1.0 mol/L sulfuric acid solution at 130 °C, and the results are shown in Fig. 10. The OCP almost kept at a quasi-steady state, and value of OCP was increased with an increase of oxygen partial pressure, as shown in Fig. 10(a). The OCP (φ_{CuFeS_2}) can be presented as [40]

$$\varphi_{CuFeS_2} = \varphi_{const} + n\lg[Ox]/[Red] \quad (12)$$

where φ_{CuFeS_2} is OCP (V); φ_{const} is the potential of chalcopyrite when [Ox]=[Red] (V); n is the slope of line in the leaching system $\varphi_{CuFeS_2} = f(\lg[Ox]/[Red])$; [Ox] is the oxidant concentration (mol/L); [Red] is reductant concentration (mol/L). As mentioned above, the explanation for the change of OCP is attributed to the increasing amount of available oxygen in the solution, which caused by the increase of oxygen partial pressure.

Figure 10(b) shows the potentiodynamic curves for the chalcopyrite electrode in 1.0 mol/L sulfuric acid solution with different oxygen partial pressures at a potential sweep rate of 1.0 mV/s. For the electrolyte with saturated vapor pressure, the potentiodynamic curve shows significantly different φ−I profiles from that with the oxygen partial pressure of 0.4 MPa, suggesting that chalcopyrite dissolution with different oxygen partial pressures had different electrochemical mechanisms. According to the mixed potential theory, as shown in Fig. 10(c), the cathodic reaction rate increased with the increase of oxygen partial pressure, resulting in the increase of φ_{ccor} and I_{corr}.

From the potentiodynamic curve obtained with saturated vapor pressure, a clear passive region from the OCP to approximately 0.4 V could be

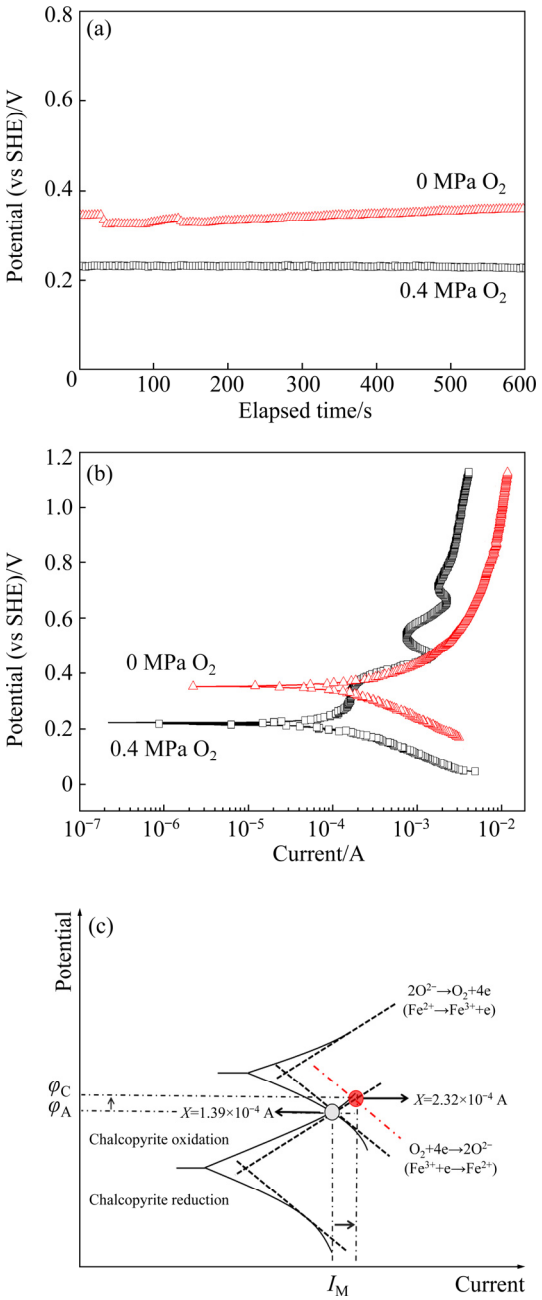

Fig. 10 Time−potential relationships (a) and potentiodynamic curves (b) of chalcopyrite electrodes at 130 °C, and mixed potential theory (c)

related to elemental sulfur formation, as presented by Reaction (1). A trans-passive dissolution occurred at potential values of 0.4−0.5 V, which can be attributed to the oxidation of elemental sulfur at higher potential [41]. As the anodic potential reached 0.5 V, the electrode transformed into the passivation region characterized by a decrease in the current density via Reaction (13), which was consistent with the research reported by HACKL et al [6]. As the potential reached above 0.6 V, the previously formed surface layer ($Cu_{1-x}Fe_{1-y}S_2$)

transformed into another layer, as shown in Reaction (14) [42]. When potential was increased above 0.65 V, the most probable reactions were the transform of $Cu_{1-x-y}S_2$ and the dissolution of chalcopyrite via Reactions (15) and (16) [6,43]. The anodic current density decreasing over a range of 0.65−0.70 V could be related to the layer of elemental sulfur, which was formed during the conversion of previously formed $Cu_{1-x-y}S_2$ layer:

$$CuFeS_2 + 4H_2O \rightarrow Cu_{1-x}Fe_{1-y}S_2 + xCu^{2+} + yFe^{3+} + zSO_4^{2-} + 8zH^+ + (2x+3y+6z)e \quad (13)$$

$$Cu_{1-x}Fe_{1-y}S_2 \rightarrow Cu_{1-x-z}S_2 + zCu^{2+} + (1-y)Fe^{2+} + 2(z+1-y)e \quad (14)$$

$$Cu_{1-x-z}S_2 \rightarrow (1-x-z)Cu^{2+} + 2S^0 + 2(1-x-z)e \quad (15)$$

$$CuFeS_2 + 8H_2O \rightarrow Cu^{2+} + Fe^{3+} + 2SO_4^{2-} + 16H^+ + 17e \quad (16)$$

For the electrolyte with oxygen partial pressure of 0.4 MPa, the current density increased significantly in the range of OCP−0.5 V, which is related to the dissolution process of chalcopyrite oxidation, as shown in Reaction (5). As potential increased further, the active−passive and passive−transpassive transition could be related to the formation and oxidation of intermediates or the diffusion of the products.

Due to the passivation of chalcopyrite, the corrosion current density was calculated by extrapolating the cathodic linear Tafel line. The value of corrosion current density was increased from 1.39×10^{-4} to 2.32×10^{-4} A/cm^2 when the oxygen partial pressure increased to 0.4 MPa, indicating that increasing oxygen partial pressure could promote the leaching kinetics of chalcopyrite. The cathodic reaction rate significantly increased when the oxygen partial pressure increased to 0.4 MPa, and the passivation of chalcopyrite was greatly weakened with the increase of the oxygen partial pressure.

3.6.2 EIS measurements with different oxygen partial pressures

EIS was used to study the chalcopyrite pressure leaching mechanism with different oxygen partial pressures, as demonstrated in Fig. 11. Based on the previous electrochemical studies, the electrical equivalent circuit $R_s(Q_1(R_1(Q_2R_2)))$ was used to fit the impedance data [41,44], and the corresponding electrical equivalent circuit is shown in Fig. 11(a). R_s is the resistance of the solution. R_1 and R_2 correspond to the charge transfer resistance of chalcopyrite oxidation and the resistance of the passive film, respectively. Table 2 shows the fitting results for different oxygen partial pressures. The value of R_2 is much larger than R_1, suggesting that the formation of passive film played an important role in chalcopyrite dissolution. As the oxygen partial pressure increased to 0.4 MPa, the values of R_1 and R_2 decreased to 2.88 and 78.91 Ω·cm^2, respectively, which were much lower than the values at saturated vapor pressure. Considering the XRD results, it can be concluded that the diffusion of the oxidan (O_2 or Fe^{3+}) was an important factor affecting the chalcopyrite leaching process, and elemental sulfur (S^0) was the main passivation product at lower oxygen partial pressure.

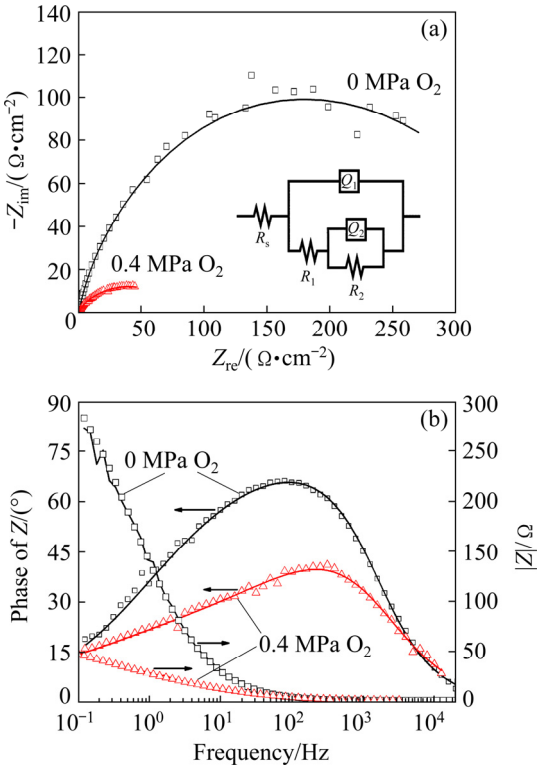

Fig. 11 Nyquist plots (a) and Bode plots (b) of chalcopyrite at 130 °C (H_2SO_4 concentration: 1.0 mol/L, scan rate: 1.0 mV/s)

3.6.3 Electron microprobe study

Electron microprobe analysis was used to determine the chemical composition of the chalcopyrite electrode dissolved at OCP with 0.4 MPa oxygen partial pressure for 60 min, and the results are shown in Fig. 12. The sulfur content on

the electrode surface was much higher than that of copper and iron, which is consistent with the results of XRD and XPS analysis.

3.6.4 XPS study

According to the above analysis, the product layers would hinder the dissolution of chalcopyrite, and it was reported that the thickness of the passivation layer was less than 5 nm [45]. XPS measurements were used to study the chemical compositions and elemental valence states of the electrodes after dissolution in 1.0 mol/L sulfuric acid solution with different oxygen partial pressures for 60 min, as shown in Fig. 13.

Figure 13(a) shows the Cu 2p spectrum of the chalcopyrite ore and leached chalcopyrite. The Cu 2p spectra displayed two strong peaks at about 932.0 and 952.1 eV, which represented Cu $2p_{3/2}$ and Cu $2p_{1/2}$, respectively, suggesting the presence of Cu(I)—S [27,46]. Figure 13(b) shows the Fe 2p spectra of the chalcopyrite ore and leached chalcopyrite. The species of iron in the un-leached chalcopyrite included Fe(III)—O/OH and iron sulphide species. The peak with the binding energy of 707.3 eV was related to the Fe $2p_{3/2}$ of Fe(III)—S. In consideration of the presence of Cu(I)—S (Fig. 13(a)) and the peak at 161.1 eV in the S 2p spectrum (Fig. 13(c)), chalcopyrite was confirmed by comparing the binding energies. However, no evidence for Fe 2p3/2 peak existed on the surface of electrode after dissolution, which might be attributed to the formation of elemental sulfur and the copper-rich polysulfide $Cu_{1-x}S$.

In order to further confirm the sulfur valence states and the chemical compositions of the passive layer, a series of high-resolution spectra of S 2pspectra for chalcopyrite samples are shown in Fig. 13(c). The binding energy at 161.3 eV was attributed to S $2p_{3/2}$ of monosulfide (S^{2-}). The S $2p_{3/2}$ core level peak with the binding energy of about 162.2 eV matched well with S $2p_{3/2}$ peak position of disulfide (S_2^{2-}), which was related to the chemical bonds of Cu—S and Fe—S in the metal-deficient sulphide phase ($Cu_{1-x}Fe_{1-y}S_2$). The

Table 2 EIS fitting results for chalcopyrite leached at different oxygen partial pressures

Oxygen partial pressure/MPa	R_s/(Ω·cm^2)	$Y_{0.1}$	n_1	R_1/(Ω·cm^2)	$Y_{0.2}$	n_2	R_2/(Ω·cm^2)
0	0.88	4.76×10^{-4}	0.85	37.1	1.79×10^{-3}	0.39	423.3
0.4	1.11	6.42×10^{-4}	0.78	2.88	1.26×10^{-2}	0.35	78.91

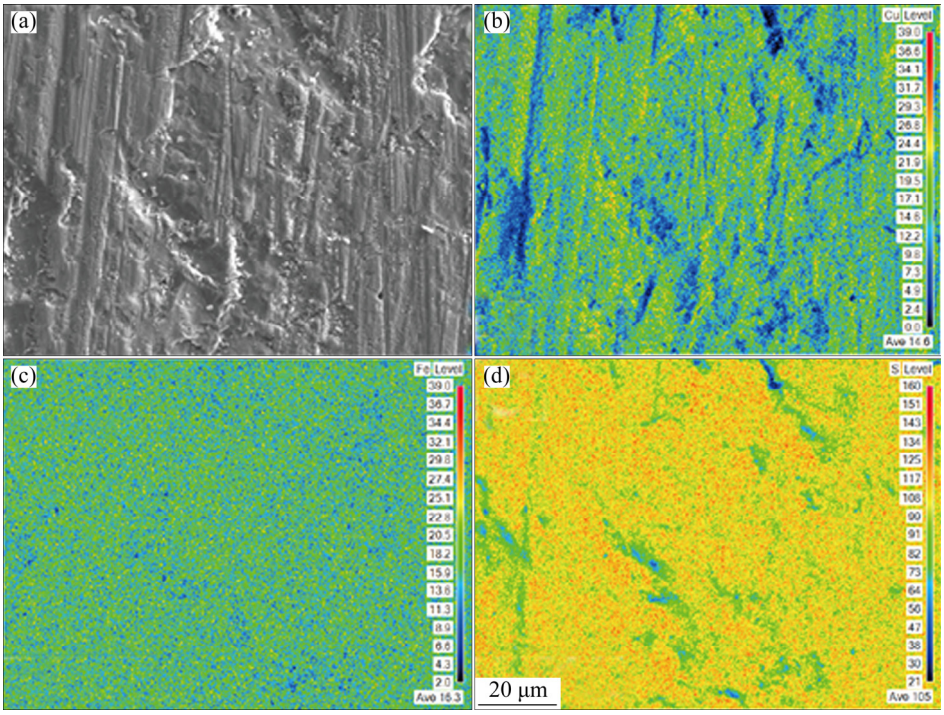

Fig. 12 Backscattered electron image (a) and electron microprobe results of copper (b), iron (c) and sulfur (d) of chalcopyrite electrode surface after being leached at OCP with 0.4 MPa oxygen partial pressure for 60 min

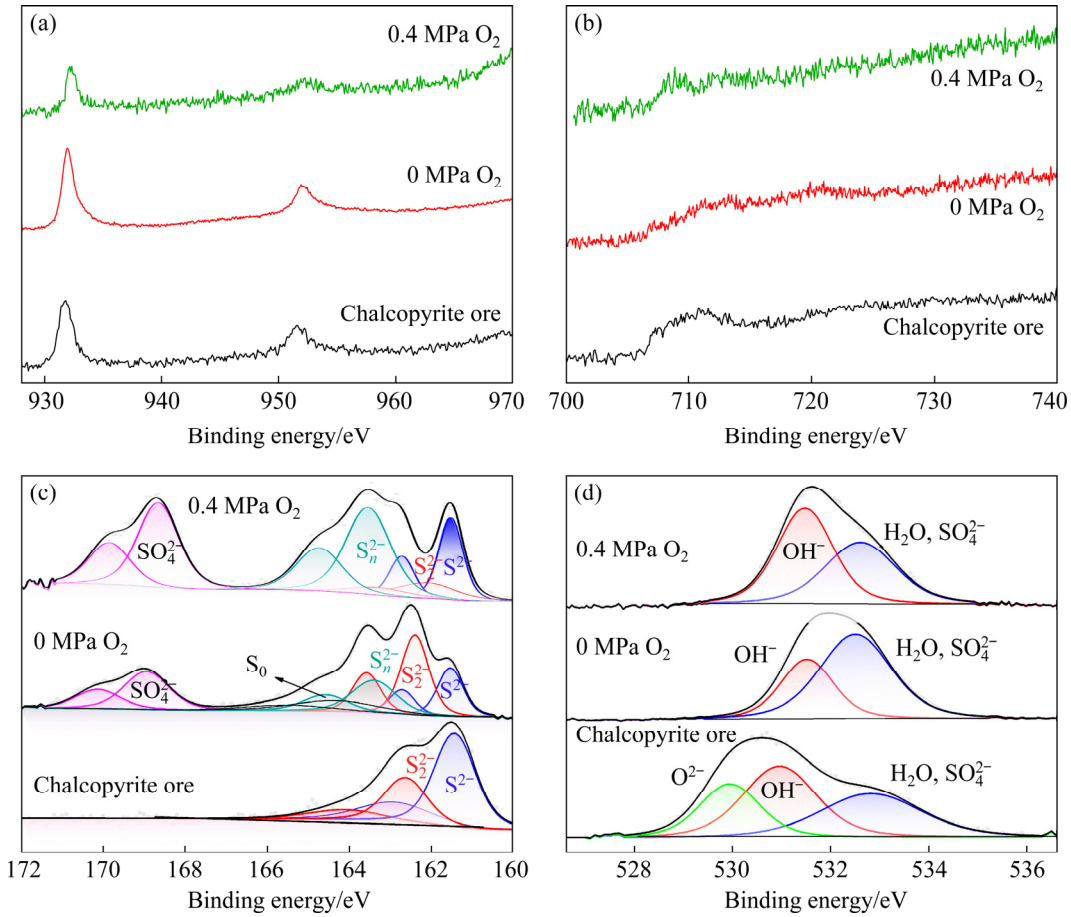

Fig. 13 XPS spectra of Cu 2p (a), Fe 2p (b), S 2p (c) and O 1s (d) of chalcopyrite electrode after dissolution in 1.0 mol/L sulfuric acid solution with different oxygen partial pressures for 60 min

S $2p_{3/2}$ peak at about 163.2 eV could be caused by the existence of polysulfide (S_n^{2-}, n>2). The peaks of monosulfide (S^{2-}) in all S 2p spectra could be attributed to the S $2p_{3/2}$ of chalcopyrite [47]. The peak of elemental sulfur was obvious in S 2p spectra of chalcopyrite after dissolution without oxygen partial pressure, which was consistent with XRD results. Interestingly, S 2p spectra of leaching residue with oxygen partial pressure of 0.4 MPa showed a disappearance of sulfur, which was related to the oxidation of elemental sulfur at higher oxygen partial pressure. The results showed that the elemental sulfur was the main component of passive layer under low oxygen partial pressure, while copper-rich sulphide was the main component of the passive layer at higher oxygen partial pressure.

Figure 13(d) shows the XPS spectra of O 1s of chalcopyrite samples. The peak at 529.6 eV corresponded to O^{2-} in oxide and adsorbed oxygen. The peak at 531.5 eV was related to OH^- in hydroxide species ($H_3O(Fe(SO_4)_2(OH)_6)$), which were detected in the leaching residue by HAN et al [24]. The peak at high binding energy of 532.8 eV could be attributed to oxygen in sulfate or water. The concentration of sulfate or adsorbed water increased as oxygen partial pressure increased, and the O^{2-} peak disappeared after leaching. The peak area at the binding energy of 531.5 eV was increased with the increase of oxygen partial pressure, as shown in Fig. 13(d), which might be caused by the oxidation of ferrous iron to ferric iron. Hence, it can be confirmed that some hydroxide species, such as jarosite, might be formed on the surface of the residue leached with high oxygen partial pressure.

4 Conclusions

(1) The chalcopyrite leaching rate increased with the increase of temperature from 120 to 150 °C. Increasing oxygen partial pressure accelerated chalcopyrite leaching. The release of iron into solution was faster than that of copper. Intermediate

iron-depleted sulfides layer (e.g. $Cu_{1-x}Fe_{1-y}S_{2-z}$, $Cu_{1-x}S$) was formed, which mixed with elemental sulfur to form passive layers on chalcopyrite surface. The leaching process was controlled by the surface reaction and product layer diffusion with an activation energy of 36.61 kJ/mol.

(2) XRD, SEM and XPS analysis revealed that elemental sulfur was the main leaching product. Calcium lignosulphonate could be used as a useful sulfur dispersing agent to solve sulfur passivation problem. Pressure leaching with calcium lignosulphonate was controlled by chemical reactions, and the activation energy was 45.49 kJ/mol.

(3) Electrochemical studies indicated that increasing oxygen partial pressure had a significant effect on both cathodic and anodic reaction kinetics. With the increase of oxygen partial pressure, the corrosion current density increased from 1.39×10^{-4} to 2.32×10^{-4} A/cm^2. The charge transfer resistance of chalcopyrite oxidation and the resistance of the passive film were both decreased with the increase of oxygen partial pressure, indicating that increasing oxygen partial pressure promoted the leaching of chalcopyrite by accelerating the electrochemical process and weakening the influence of passive film.

Acknowledgments

This work was supported by the National Natural Science Foundation of China (Nos. 51574072, 51434001), and the Fundamental Research Funds for the Central Universities, China (No. 2025028).

References

[1] SCHIPPER B W, LIN H C, MELONI M A, WANSLEEBON K, HEIJUNGA R, VOET E. Estimating global copper demand until 2100 with regression and stock dynamics [J]. Resources, Conservation and Recycling, 2018, 132: 28−36. doi.org/10.1016/j.resconrec.2018.01.004.

[2] ELSHKAKI A, GRAEDEL T E, CIACCI L, RECK B. Copper demand, supply, and associated energy use to 2050 [J]. Global Environmental Change, 2016, 39: 305−315. doi.org/ 10.1016/j.gloenvcha.2016.06.006.

[3] OLUBAMI P A, POTGIETER J H. Investigations on the mechanisms of sulfuric acid leaching of chalcopyrite in the presence of hydrogen peroxide [J]. Mineral Processing and Extractive Metallurgy Review, 2009, 30: 327−345. doi.org/ 10.1080/08827500902958191.

[4] CHEN Ming-lian, ZHANG Lin, GU Guo-hua, HU Yue-hua, SU Li-jun. Effects of microorganisms on surface properties of chalcopyrite and bioleaching [J]. Transactions of Nonferrous Metals Society of China, 2008, 18: 1421−1426. doi.org/10.1016/S1003-6326(09)60019-4.

[5] CÓRDOBA E M, MUÑOZ J A, BLÁZQUEZ M L,GONZÁLEZ F, BALLESTER F. Passivation of chalcopyrite during its chemical leaching with ferric ion at 68 °C [J]. Minerals Engineering, 2009, 22: 229−235. doi.org/10.1016/j.mineng.2008.07.004.

[6] HACKL R P, DREISINGER D B, PETERS E, KING J A. Passivation of chalcopyrite during oxidative leaching in sulfate media [J]. Hydrometallurgy, 1995, 39: 25−48. doi.org/10.1016/0304-386X(95)00023-A.

[7] XIAN Y J, WEN S M, DENG J S, LIU Q, NIE J. Leaching chalcopyrite with sodium chlorate in hydrochloric acid solution [J]. Canadian Metallurgical Quarterly, 2013, 51: 133−140. doi.org/10.1179/1879139512Y.0000000001.

[8] WU Jia-jia, AHN J, LEE J. Kinetic and mechanism studies using shrinking core model for copper leaching from chalcopyrite in methanesulfonic acid with hydrogen peroxide [J]. Mineral Processing and Extractive Metallurgy Review, 2020, 2: 1−8. doi.org/10.1080/08827508.2020.1795850.

[9] QIU Ting-sheng, NIE Guang-hua, WANG Jun-feng, CUI Li-feng. Kinetic process of oxidative leaching of chalcopyrite under low oxygen pressure and low temperature [J]. Transactions of Nonferrous Metals Society of China, 2007, 17: 418−422. doi.org/10.1016/S1003-6326(07) 60108-3.

[10] GONZALO V G, MARYCARMEN M, PEN G, DIXON D G. Electrochemical hysteresis and bistability in chalcopyrite passivation [J]. Hydrometallurgy, 2010, 105: 140−147. doi.org/10.1016/j.hydromet.2010.08.012.

[11] KARTAL M, XIA Fang, RALPH D, RICKARD W, REBARD F, LI Wei. Enhancing chalcopyrite leaching by tetrachloroethylene-assisted removal of sulphur passivation and the mechanism of jarosite formation [J]. Hydrometallurgy, 2020, 191: 105192. doi.org/10.1016/j. hydromet.2019.105192.

[12] WU Shi-fa, YANG Cong-ren, QIN Wen-qing, JIAO Fen, WANG Jun, ZHANG Yan-sheng. Sulfur composition on surface of chalcopyrite during its bioleaching at 50 °C [J] Transactions of Nonferrous Metals Society of China, 2015, 25: 4110−4118. doi.org/10.1016/S1003-6326(15) 64062-6.

[13] HACKL R P, DREISINGER D B, PETERS E, KING J A. Passivation of chalcopyrite during oxidative leaching in sulfate media [J]. Hydrometallurgy, 1995, 39: 25−48. doi. org/10.1016/0304-386X(95)00023-A.

[14] STOTT M B, WATLING H R, FRANZMANN P D, SUTTON D. The role of iron-hydroxy precipitates in the passivation of chalcopyrite during bioleaching [J]. Minerals Engineering, 2000, 13: 1117−1127. doi.org/10.1016/S0892-6875(00)00095-9.

[15] O'CONNOR G M, EKSTEEN J J. A critical review of the passivation and semiconductor mechanisms of chalcopyrite leaching [J]. Minerals Engineering, 2020, 154: 106401. doi.org/ 10.1016/j.mineng.2020.106401.

[16] YIN Q, VAUGHAN D J, ENGLAND K E R, KELSALL G H, BRANDON N P. Surface oxidation of chalcopyrite ($CuFeS_2$) in alkaline solutions [J]. Journal of the Electrochemical Society, 2000, 147: 2945−2951. doi.org/10. 1149/1.1393629.

[17] İKİZ D, GÜLFEN M, AYDIN A O. Dissolution kinetics of primary chalcopyrite ore in hypochlorite solution [J]. Minerals Engineering, 2006, 19: 972−974. doi.org/10.1016/j.mineng.2005.09.047.

[18] CHÁIDEZ J, PARGA J, VALENZUELA J, CARRILLO R, ALMAGUER I. Leaching chalcopyrite concentrate with oxygen and sulfuric acid using a low-pressure reactor [J]. Metals−Open Access Metallurgy Journal, 2019, 9(2): 189. doi.org/10.3390/met9020189.

[19] BABA A A, GHOSH M K, PRADHAN S R, RAO D S, BARAL A, ADEKOLA F A. Characterization and kinetic study on ammonia leaching of complex copper ore [J]. Transactions of Nonferrous Metals Society of China, 2014, 24: 1587−1595. doi.org/10.1016/S1003-6326(14)63229-5.

[20] PETROVIĆ S J, BOGDANOVIĆ G D, MANTONIJEVIĆ M. Leaching of chalcopyrite with hydrogen peroxide in hydrochloric acid solution [J]. Transactions of Nonferrous Metals Society of China, 2018, 28: 1444−1455. doi.org/10.1016/S1003-6326(18)64788-0.

[21] MCDONALD R G, MUIR D M. Pressure oxidation leaching of chalcopyrite. Part I: comparison of high and low temperature reaction kinetics and products [J]. Hydrometallurgy, 2007, 86: 191−205. doi.org/10.1016/j.hydromet.2006.11.015.

[22] TURAN M D, SAR Z A, NIZAMOLU H. Pressure leaching of chalcopyrite with oxalic acid and hydrogen peroxide [J]. Journal of the Taiwan Institute of Chemical Engineers, 2021, 118: 112−120. doi.org/10.1016/j.jtice.2020.10.021.

[23] YU P H, HANSEN C K, WADSWORTH M E. A kinetic study of the leaching of chalcopyrite at elevated temperatures [J]. Metallurgical Transactions, 1973, 4: 2137−2144. doi.org/10.1007/BF02643279.

[24] HAN B, ALTANSUKH B, HAGA K, TAKASAKI Y. Leaching and kinetic study on pressure oxidation of chalcopyrite in H_2SO_4 solution and the effect of pyrite on chalcopyrite leaching [J]. Journal of Sustainable Metallurgy, 2017, 3: 528−542. doi.org/10.1007/s40831-017-0135-3.

[25] HEGURI S, ASANO S, LDEGAMI A. Behavior of iron and sulfur in the pressure leaching of chalcopyrite [J]. Journal of MMIJ, 2015, 131: 470−475. doi.org/10.2473/journalofmmij.131.470.

[26] CUI Can, LI He-ping, LIN Sen, WANG Pan. In situ electrochemical investigation of acidic pressure oxidation of pyrite at 160−240 °C [J]. Journal of the Electrochemical Society, 2018, 165: c289−c294. doi.org/10.1149/2.0081807jes.

[27] GHAHREMANINEZHAD A, DIXON D G, ASSELIN E. Electrochemical and XPS analysis of chalcopyrite ($CuFeS_2$) dissolution in sulfuric acid solution [J]. Electrochimica Acta, 2013, 87: 97−112. doi.org/10.1016/j.electacta.2012.07.119.

[28] LI Shuang-ke, GU Guo-hua, QIU Guan-zhou, CHEN Zhi-xiang. Flotation and electrochemical behaviors of chalcopyrite and pyrite in the presence of *N*-propyl-*N*′-ethoxycarbonyl thiourea [J]. Transactions of Nonferrous Metals Society of China, 2018, 28: 1241−1247. doi.org/10.1016/S1003-6326(18)64762-4.

[29] DIGBY D, MACDONALD. Silver-silver chloride thermocells and thermal liquid junction potentials for potassium chloride solutions at elevated temperatures [J]. Journal of the Electrochemical Society, 1979, 126: 1618−1624. doi.org/10.1149/1.2129342.

[30] LU Dian-kun, WANG Wei, CHANG Yong-feng, XIE Feng, JIANG Kai-xi. Thermodynamic analysis of possible chalcopyrite dissolution mechanism in sulfuric acidic aqueous solution [J]. Metals, 2016, 6: 303−318. doi.org/10.3390/met6120303.

[31] BUCKLEY A N, WOODS R. An X-ray photoelectron spectroscopic study of the oxidation of chalcopyrite [J]. Australian Journal of Chemistry, 1984, 37: 2403−2413. doi.org/10.1071/CH9842403.

[32] ALEKSEI K, STANISLAV N, KIRILL K, AGARWAL V, LUNDSTRÖM M. Hydrothermal pretreatment of chalcopyrite concentrate with copper sulfate solution [J]. Hydrometallurgy, 2020, 195: 105539. doi.org/10.1016/j.hydromet.2020.105359.

[33] WANG L, ZHOU W, SONG S, GAO H, AI G. Selective separation of hematite from quartz with sodium oleate collector and calcium lignosulphonate depressant [J]. Journal of Molecular Liquids, 2021, 322: 114502. doi.org/10.1016/j.molliq.2020.114502.

[34] EDVARDSSON K, MAGNUSSON R. Impact of fine materials content on the transport of dust suppressants in gravel road wearing courses [J]. Journal of Materials in Civil Engineering, 2011, 23: 1163−1170. doi.org/10.1061/(ASCE)MT.1943-5533.0000282.

[35] HACKL R P, DREISINGER D B, KING J A. Effect of sulfur dispersing surfactants on the oxygen pressure leaching of chalcopyrite [C]//COOPER W C, DREISINGER D B, DUTRIZAC J E, HEIN H, UGARTE G. Proceedings of Copper 95–Cobre 95 International Conference−Electrorefining and Hydrometallurgy of Copper. Vol. 3. The Metallurgical Society of CIM, Montreal, Canada, 1995: 559−577.

[36] TONG L, DREISINGER D. Interfacial properties of liquid sulfur in the pressure leaching of nickel concentrate [J]. Minerals Engineering, 2009, 22: 456−461. doi.org/10.1016/j.mineng.2008.12.003.

[37] MA Jia-yu, DU Xue-lan, QIN Yuan-hang, WU Zai-kun, CHI Ru-an. Kinetics on leaching of potassium from phosphorus-potassium associated ore in $HCl-H_3PO_4$ media [J]. Transactions of Nonferrous Metals Society of China, 2017, 27: 1870−1877. doi.org/10.1016/S1003-6326(17)60211-5.

[38] DREISINGER D, ABED N. A fundamental study of the reductive leaching of chalcopyrite using metallic iron part I: kinetic analysis [J]. Hydrometallurgy, 2002, 66: 37−57. doi.org/10.1016/S0304-386X(02)00079-8.

[39] LIU Zhi-xiong, XIANG Yan-hong, YIN Zhou-lan, WU Xian-wen, JIANG Jian-bo, CHEN Yi-guang, XIONG Li-zhi. Oxidative leaching behavior of metalliferous black shale in acidic solution using persulfate as oxidant [J]. Transactions of Nonferrous Metals Society of China, 2016, 26: 565−574. doi.org/10.1016/S1003-6326(16)64145-6.

[40] LIU Q Y, CHEN M, YANG Y. The effect of chloride ions on the electrochemical dissolution of chalcopyrite in sulfuric acid solutions [J]. Electrochimica Acta, 2017, 253: 257−267. doi.org/10.1016/j.electacta.2017.09.063.

[41] GHAHREMANINEZHAD A, ASSELIN E, DIXON D G. Electrochemical evaluation of the surface of chalcopyrite

during dissolution in sulfuric acid solution [J]. Electrochimica Acta, 2010, 55: 5041−5056. doi.org/10.1016/j.electacta.2010.03.052.

[42] PARKER A J, PAUL R L, POWER G P. Electrochemistry of the oxidative leaching of copper from chalcopyrite [J]. Journal of Electroanalytical Chemistry and Interfacial Electrochemistry, 1981, 118: 305−316. doi.org/10.1016/S0022-0728(81)80549-9.

[43] LAZARP I, NICOL M J. A rotating ring-disk study of the initial stages of the anodic dissolution of chalcopyrite in acidic solutions [J]. Journal of Applied Electrochemistry, 2006, 36: 425−431. doi.org/10.1007/s10800-005-9089-4.

[44] ASSELIN E, ALFANTAZI A, ROGAK S. Effect of oxygen on the corrosion behavior of alloy 625 from 25 to 200 °C [J]. Journal of the Electrochemical Society, 2007, 154(4): 215−229. doi.org/10.1149/1.2435620.

[45] YIN Q, KELSALL G, VAUGHAN D, ENGHLANG K. Atmospheric and electrochemical oxidation of the surface of chalcopyrite ($CuFeS_2$) [J]. Geochimica et Cosmochimica Acta, 1995, 59: 1091−1100. doi.org/10.1016/0016-7037(95)00026-V.

[46] NAKAI I, SUGITANI Y, NAGASHIMA K, NIWA Y. X-ray photoelectron spectroscopic study of copper minerals [J]. Journal of Inorganic and Nuclear Chemistry, 1978, 40: 789−791. doi.org/10.1016/0022-1902(78)80152-3.

[47] YANG Hong-ying, GONG En-pu, YANG Li, CHEN Gang, FAN You-jing, ZHAO Yu-shan, LU Jiu-ji. XPS characteristics of sulfur of bio-oxidized arsenic-bearing gold concentrate and changes of surface nature of bio-oxidation residue [J]. Transactions of Nonferrous Metals Society of China, 2004, 14: 1187−1191. doi.org/ 10.1016/j.scriptamat.2004.07.003.

温度、氧分压和木质素磺酸钙对黄铜矿在硫酸溶液中加压氧化浸出的影响

白云龙[1,2]，王 伟[1,2]，谢 锋[1,2]，路殿坤[1,2]，蒋开喜[3]

1. 东北大学 多金属共生矿生态化冶金教育部重点实验室，沈阳 110819；
2. 东北大学 冶金学院，沈阳 110819；
3. 福州大学 紫金矿业学院，福州 350108

摘 要：采用浸出实验和原位电化学测试研究黄铜矿加压浸出机理，考察浸出温度、氧分压和木质素磺酸钙对铜和铁浸出的影响。结果表明，当浸出温度从 120 ℃升高到 150 ℃、增加氧分压至 0.7 MPa 时，黄铜矿的浸出速率增大。贫铁硫化物在黄铜矿表面的形成导致铁比铜更快浸出。在无木质素磺酸钙添加条件下，铜的浸出率为 79%，铁的浸出率为 81%，浸出过程受化学反应和产物层扩散混合控制，活化能为 36.61 kJ/mol。木质素磺酸钙可以有效改善硫的钝化问题，浸出过程受表面化学反应控制，活化能为 45.59 kJ/mol。元素硫是主要的浸出产物，与贫铁硫化物共同导致“钝化现象”。电化学研究表明，增加氧分压能加速阴极反应速率并减弱黄铜矿的“钝化”，从而提升黄铜矿浸出速率。

关键词：黄铜矿；加压氧化浸出；木质素磺酸钙；动力学；电化学

(Edited by Bing YANG)